Impact of inlet channel geometry on microfluidic drop formation

A. R. Abate,[1] A. Poitzsch,[2] Y. Hwang,[3] J. Lee,[4] J. Czerwinska,[5] and D. A. Weitz[1]

[1]*Department of Physics and SEAS, Harvard University, Cambridge, Massachusetts 02138, USA*

[2]*Pinkerton Academy, Derry, New Hampshire 03038, USA*

[3]*St. Paul's School, Concord, New Hampshire 03301, USA*

[4]*Lexington High School, Lexington, Massachusetts 02421, USA*

[5]*IPPT PAN, Polish Academy of Sciences, Swietokrzyska 21, PL 00-049 Warszawa, Poland*

We study the impact of inlet channel geometry on microfluidic drop formation. We show that drop makers with T-junction style inlets form monodisperse emulsions at low and moderate capillary numbers and those with Flow-Focus style inlets do so at moderate and high capillary numbers. At low and moderate capillary number, drop formation is dominated by interfacial forces and mediated by the confinement of the microchannels; drop size as a function of flow-rate ratio follows a simple functional form based on a blocking-squeezing mechanism. We summarize the stability of the drop makers with different inlet channel geometry in the form of a phase diagram as a function of capillary number and flow-rate ratio.

PACS number(s): 47.15.Fe, 47.15.Rq, 47.20.Ma, 47.57.jb

Microfluidic drop formation is important for a variety of applications [1,2], for performing chemical reactions and for making drops that can be used as templates for the synthesis of materials with novel properties [3–14]. Flow-focus drop formation can be used to exert precise forces on fluids and objects at the microscale to measure their microrheology; this is a very accurate way to measure the extensional shear viscosity of a fluid [15]. The drops can also be used as microreactors within which to perform individual biological assays [16–21]. The microreactor drops can be formed, merged, and sorted continuously in an assembly-line process at kilohertz rates [22]. This combination of speed, containment, and small volumes is very useful for high-throughput screening, for the discovery of new drugs and for the directed evolution of enzymes and cells [23–30].

In microfluidics there are two dominant classes of drop makers, each having distinctive inlet channel geometry: T-junction (TJ) [31–35] and flow-focus (FF) [36–42] drop makers. Whereas TJ drop makers use two inlets, FF drop makers use three inlets and a symmetric junction. These differences lead to differences in performance and in the properties of the drops that are produced; however, a direct comparison of these drop makers under the same experimental conditions has not been performed. This can make choosing the best geometry for the application difficult; often, a geometry is chosen arbitrarily and tested by trial and error. A superior method would be to understand intrinsic differences between drop makers and to select the best one based on this knowledge.

In this paper, we present a direct comparison of microfluidic drop makers with a different inlet channel geometry. We study several variations in TJ and FF drop makers and introduce a geometry we dub pinned-jet-flow focusing (PJFF). We show that the geometry of the inlet channels of microfluidic drop makers influences the range of capillary numbers and flow-rate ratios over which monodisperse emulsions can be formed. For example, in TJ and PJFF drop formation, the asymmetric injection of fluids leads to a stable drop formation at low capillary numbers and jetting at high capillary numbers. By contrast, in FF drop formation, the symmetric injection leads to unstable polydisperse drop formation at low capillary numbers and monodisperse drop formation at high capillary numbers. At low and moderate capillary numbers (Ca < 0.05), drop formation is dominated by interfacial forces and mediated by the geometrical confinement of the microchannels and proceeds through a blocking-squeezing process [35]. In this regime, drop size as a function of flow-rate follows a simple linear functional form. We summarize the stability of different drop makers in the form of a phase diagram for stable drop formation as a function of capillary number and flow-rate ratio.

The microfluidic drop makers are fabricated using soft lithography in poly(dimethylsiloxane) [43]. All devices consist of poly(dimethylsiloxane) (PDMS) channels that are bonded to a glass slide and have a fixed channel height of 15 μm. The drop makers consist of multiple inlet channels that drain into a single nozzle channel, where drops are formed. The nozzle channels for all drop makers have fixed dimensions of 15×15 μm^2; by holding the nozzle channel dimensions constant, we perform an isolated study of the importance of inlet channel geometry. To enable production of water-in-oil emulsions, we treat the channels with Aquapel glass treatment (Pittsburgh Glass Works), which makes the PDMS channels and bottom glass plate very hydrophobic. After the application of Aquapel, the channels have a water-in-air contact angle of $>105°$ and a fluorocarbon oil-in-air contact angle of $<3°$. For the droplet phase, we use distilled water having kinematic viscosity 0.9 cSt and density 1000 kg/m^3. For the continuous phase, we use HFE-7500 fluorocarbon oil having kinematic viscosity 0.77 cSt and density 1614 kg/m^3. The water-in-oil emulsions are stabilized by the fluorosurfactant ammonium carboxylate of Krytox 157 FSL (Dupont). We synthesize the fluorosurfactant by dissolving 20 g of Krytox 157 FSL in 180 g methanol. We then add ~0.6 g concentrated ammonium hydroxide drop wise until the solution clears. The residual methanol and ammonia are then evaporated, producing a clear viscous liquid which is ready for use. To use, we dissolve the surfactant in HFE-7500 at 1.8% by weight. The surface tension between the water and HFE-7500 fluorocarbon oil with surfactant is
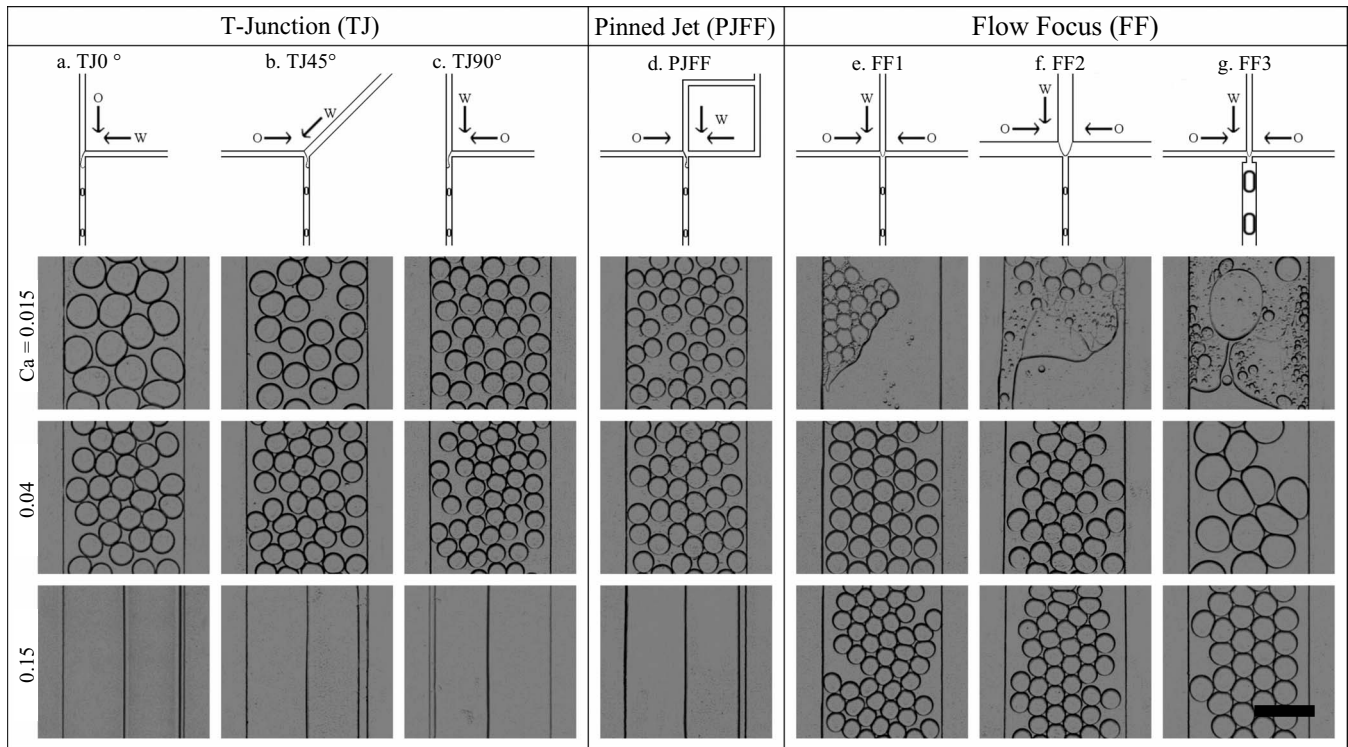
FIG. 1. Schematics of drop makers with different inlet channel geometries (top row). The drop maker nozzle channel dimensions for all devices are constant, with cross-sectional dimensions 15×15 μm^2. The emulsions formed consist of water drops in fluorocarbon oil stabilized by fluorosurfactant. Example images of drops formed by each device for the flow-rate ratio of 1:1 and different capillary number are shown in the lower rows: for capillary number of 0.015 (second row), 0.04 (third row), and 0.15 (fourth row). The scale bar denotes 100 μm.

2–5 mN/m, as measured with a KSV Sigma 700 Tensiometer. Fluids are injected into the microfluidic devices at controlled volumetric flow rate using syringe pumps. Using these values, we compute the capillary number $Ca = \mu v / \gamma$, where v is the average speed of the continuous phase and μ is the viscosity of the oil continuous phase. To calculate v, we divide the continuous phase volumetric flow rate, which we control with a pump, by the average cross-sectional area occupied by the continuous phase in the nozzle channel; this is the total nozzle cross-sectional area times the ratio of the continuous phase flow rate to the total flow rate. We use the continuous phase viscosity and average speed for the calculation because the continuous phase shears the droplet phase to form the drops [32,34,35,39,44]. For our system, the viscosities of the droplet and continuous phases are nearly equal, so that we study the regime in which the viscosity ratio is close to 1.

Droplet properties are measured using high-speed imaging. Drop makers are imaged using an inverted microscope in bright-field mode. Images of the drop formation are recorded using a Sony XCD-V50 Firewire camera. The camera has an electronic shutter with charge-coupled device exposure duration of 10 μs. Over this duration, the ~ 20 μm drops move less than 1 μm, allowing them to be sharply imaged so that we can accurately measure their size and position. Movies of the drop formation are recorded at 30 frames per second for approximately 1 min; this image capture rate is not fast enough to observe the continuous motion of the drops but rather allows us to image new drops in each

movie frame to rapidly acquire statistics. To identify the drops in the images and measure their position and volume, we use a combination of automated image processing techniques and manual measurement. The images are first thresholded to binary such that the drops appear as bright region on a black background. The position and area of the regions are recorded. To measure the drop volume, we convert the observed bright area to a volume based on a pancake droplet shape since the drop diameter exceeds the height of the channels. To measure the drop periodicity, we measure the distance between consecutive drops when they are single file in the nozzle channel and divide by the average flow velocity, which we set with the pumps.

TJ drop makers consist of two inlet channels that intersect at the drop formation nozzle; this injects the water so that a tip protrudes into the nozzle channel where it is sheared by the oil, forming drops, as shown, for example, in Fig. 1(a). We compare three variations in TJ drop makers in which the water is injected at a different angle, as shown in Figs. 1(a)–1(c); the drops formed by the different drop makers are shown in the rows below for fixed flow-rate ratio of 1:1 and different capillary numbers. In FF drop formation, three inlets are used: the central for water and the two side inlets for oil, as shown in Figs. 1(e)–1(g). We study three variations in FF drop makers. In the first variation, we use a junction in which all three inlets have the same dimensions as the nozzle, as shown in Fig. 1(e). In the second variation, the inlets are wider than the nozzle, as shown in Fig. 1(f). In the
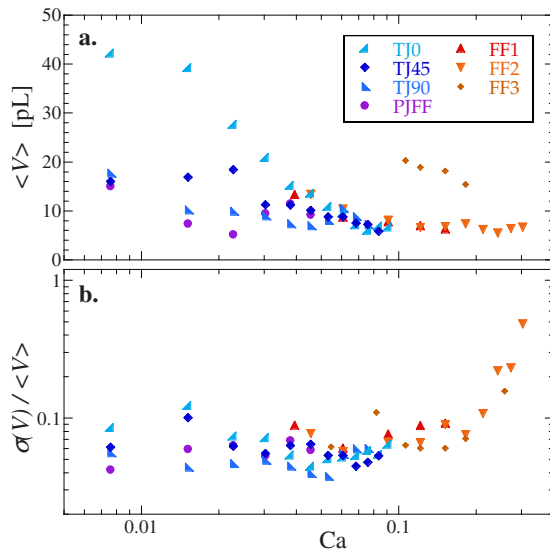
FIG. 2. (Color online) Mean (a) drop volume and (b) standard deviation divided by the mean in the drop volume as a function of capillary number for the different devices; the flow-rate ratio is held constant for all devices at $U_{out}/U_{in}=1$. The TJ and PJFF drop makers form monodisperse emulsions at low and moderate capillary number but jet at high capillary; as such, the points for these drop makers cease above 0.1. The FF drop makers are unstable at low capillary number and form monodisperse emulsions at moderate and high capillary number; as such, the points for these drop makers begin at 0.04. For moderate-low capillary number, all drop makers form drops at a similar size, rate, and monodispersity, irrespective of inlet channel geometry.

third variation, we test a common geometry in which the nozzle is short and narrow, abruptly widening from 15 to 40 μm after a 15 μm distance, as depicted in Fig. 1(g). With PJFF, we combine attributes of TJ and FF drop makers: we use three inlets but inject the water through two of the inlets, the central and one of the side inlets, as shown in the center column in Fig. 1(d). Representative images of drops formed in all devices are shown for different capillary numbers in Fig. 1. While the TJ and PJFF drop makers produce monodisperse drops at low and moderate capillary numbers, the FF drop makers do so at moderate and high capillary numbers, as shown in the top and bottom-most rows in Fig. 1. At moderate capillary numbers, all drop makers produce monodisperse drops at a similar size and rate, as shown in the middle row of images. The PJFF drop maker behaves most similarly to the TJ drop makers as a function of capillary number, as shown by comparison of the left and central columns in the figure. The FF3 drop maker behaves unlike all other drop makers, forming significantly larger drops at moderate capillary numbers, as though the effective diameter of the drop formation orifice were much larger than 15 μm, as shown in Fig. 1(g).

To quantify the dependence of the drop properties on flow conditions, we plot the average and standard deviation in the drop volumes as a function of capillary number in Fig. 2(a). For each device, we measure drop volumes only when drop formation is stable and nearly periodic. At low capillary numbers, drop formation in the FF devices is unstable, alter-

nating between jetting and short spurts of drop formation. By contrast, the TJ and PJFF drop makers are stable and produce large monodisperse drops at a periodic rate, as shown in Figs. 2(a) and 2(b). The drops from the TJ0° and TJ45° drop makers are larger than for the TJ90° and PJFF drop makers, suggesting that water injection angle influences the drop size at very low capillary numbers. As capillary number is increased, shear stresses in the nozzle increase; consequently, drop size is reduced even though flow-rate ratio is held constant at 1:1, as shown in Fig. 2(a). At these moderate capillary numbers, the FF drop maker formation begins to stabilize, producing monodisperse drops with a size and production rate that is nearly equal to that of the TJ and PJFF drop makers, as shown by the collapse of the data for all drop makers in the middle range in Fig. 2(a). As capillary number is increased further, the TJ and PJFF drop makers jet through the nozzle, flowing as parallel streams without breaking into drops; this is due to the geometry of the TJ inlet channels, which inject the water into the nozzle close to the side wall. This allows the wall to smooth out instabilities in the water/oil interface and suppress drop formation, leading to jetting [39,45–49], as is shown in the lower row of images in Figs. 1(a)–1(d) in the movies available online [50]. By contrast, in the FF drop makers the water is injected into the center of the nozzle and sheared by the oil from both sides; these devices continue to form monodisperse emulsions even at high capillary number, though there is a noticeable change in the shape of the water tip from which the drops form: whereas at low capillary number, the tip has a rounded shape and snaps back entirely to the water inlet after a drop pinches off, at high capillary number the tip has a pointed shape and remains extended into the nozzle, and the drops drip from the end (see movies available online). At still higher capillary numbers, even the FF drop makers begin to jet; shear stresses in the nozzle increase to the point at which the oil pulls long threads of water that break up into polydisperse emulsions due to Rayleigh-Plateau instabilities [44,51]; consequently, the normalized standard deviation of the drop volume increases rapidly as a function of capillary number in this range, as shown in Fig. 2(b).

To quantify the drop properties as a function of flow-rate ratio, we fix the capillary number to Ca=0.015 for the TJ drop makers and Ca=0.04 for the FF drop makers and vary the flow-rate ratio (Fig. 3). At low flow-rate ratios, we form high volume fraction emulsions consisting of large plug drops separated by short segments of oil, as demonstrated by the large drop volumes in Fig. 3(a). The plug drops are monodisperse, as shown by the low normalized standard deviation of the drop volumes in Fig. 3(b). As the ratio is increased, the drop size is reduced for all drop makers irrespective of inlet channel geometry, as shown in Fig. 3(a). As ratio is increased further, drop size is reduced only slightly while the time between drops increases and the drops remain monodisperse, as shown in Figs. 3(a) and 3(b). At these moderate-low capillary numbers, the drop formation is dominated by interfacial forces and the confinement of the microchannels [35]. Early in the drop formation cycle, the water tip extends into the nozzle, blocking it, and causing an increase in pressure in the continuous phase upstream. As the pressure increases, a neck forms in the water tip that is
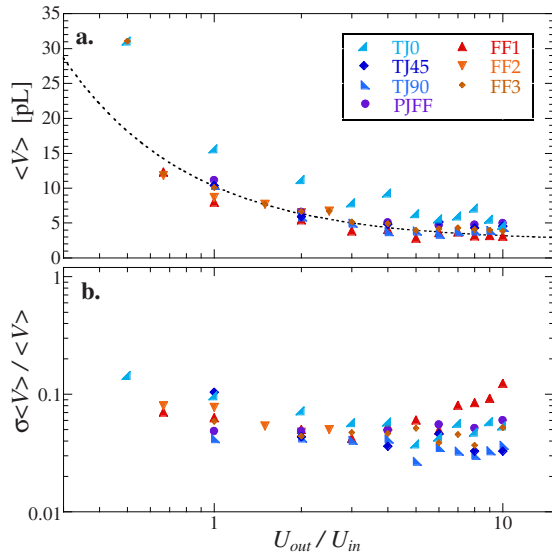
FIG. 3. (Color online) Mean (a) drop volume and (b) standard deviation divided by the mean in the drop volume as a function of flow-rate ratio; the capillary number is held constant for the TJ drop makers at Ca=0.015 and for the FF drop makers at Ca=0.04. At these moderate-low capillary number, drop formation for all devices is dominated by interfacial forces and mediated by the confinement of the microchannels. The drop volume as a function of flow-rate ratio follows the simple functional form $V \propto U_{in}/U_{out}$ (dashed black curve) [35].

FIG. 4. (Color online) Phase diagrams for stable drop formation as a function of capillary number and flow-rate ratio. (a) Schematics of the PJFF and FF2 devices. Phase diagram for (b) the PJFF device and (c) the FF2 device; the large solid symbols correspond to the boundaries between monodisperse drop formation and jetting or irregular drop formation; the small hollow symbols correspond to monodisperse drop formation. For the FF2 device, the multiple-dripping region corresponds to drop formation in which several drops of different size are formed in rapid succession in a cycle that repeats periodically [52]. (d) Overlay of the stability regions for both drop makers. Whereas the PJFF drop makers form monodisperse emulsions at lower capillary numbers and high ratios, the FF2 drop maker forms monodisperse emulsions at higher capillary numbers and lower ratios.

slowly squeezed, leading to the pinch off of a water drop [35]. This mechanism predicts a linear dependence of drop volume on flow-rate ratio, which we find to be in reasonable agreement with the measured drop volumes for all TJ, PJFF, and FF drop makers, as shown by comparison with the theoretical fit in Fig. 3(a).

The measurements of drop properties as a function of capillary number and flow-rate ratio represent two cuts through a two-dimensional phase space for stable drop formation. To map out the full phase space, we choose two representative devices and independently adjust capillary number and flow-rate ratio, while observing drop formation stability (Fig. 4). We define stable drop formation as the production of monodisperse drops at a periodic rate. The PJFF drop maker has a large region of stable drop formation, extending from low to high ratios and to very low capillary numbers, as shown in Fig. 4(b); this geometry is the best for forming monodisperse emulsions at very low capillary numbers. By contrast, the FF2 drop maker has a much smaller region of stable drop formation, unstable at all extremes so that the stable region is bounded on all sides, as shown in Fig. 4(c). Nevertheless, FF2 encapsulates an important region of the phase space not accessible to PJFF: at moderate-high capillary numbers to the middle right of the phase space, as shown by the overlay of the stability regions in Fig. 4(d). In these regions, the TJ and PJFF drop makers jet, but the FF drop makers form monodisperse drops most rapidly, useful for applications that require large quantities of drops. At the top of the FF2 diagram, the drop maker enters a multiple-dripping regime [52], forming several drops of slightly different size in rapid succession in a cycle that repeats periodically, as shown in Fig.

4(c) and in movies available online. The number of drops in the cycle can be controlled by adjusting the capillary number and flow-rate ratio [52]. We also observe this behavior for the FF1 drop maker, which has much narrower inlets, but for a much smaller range of capillary numbers and flow-rate ratios; this suggests that the ability of a drop maker to multiple drip is influenced by the geometry of the inlet channels and, specifically, the widths of the inlets with respect to the nozzle.

The geometry of the inlet channels of microfluidic drop makers influences the range of capillary numbers and flow-rate ratios over which monodisperse emulsions can be formed. Whereas TJ and PJFF drop makers form monodisperse emulsions at low and moderate capillary numbers, FF drop makers do so at moderate and high capillary numbers. A detailed understanding of drop maker performance as a function of flow conditions is important when designing microfluidic devices that use drop formation, particularly, in combination with other processes, such as merger and sorting, which can be very sensitive to flow conditions and drop properties. Our results should enable selection of the best geometry for the specific application without having to perform time-intensive prototyping experiments.

---

[1] T. M. Squires and S. R. Quake, Rev. Mod. Phys. **77**, 977 (2005).

[2] G. M. Whitesides, Nature (London) **442**, 368 (2006).

[3] Z. Nie, W. Li, M. Seo, S. Xu, and E. Kumacheva, Nano Lett. **2**, 891 (2002).

[4] A. S. Utada, E. Lorenceau, D. R. Link, P. D. Kaplan, H. A. Stone, and D. A. Weitz, Science **308**, 537 (2005).

[5] T. Nisisako, T. Torii, T. Takahashi, and Y. Takizawa, Adv. Mater. **18**, 1152 (2006).

[6] J. W. Kim, A. S. Utada, A. Fernandez-Nieves, Z. Hu, and D. A. Weitz, Angew. Chem., Int. Ed. **46**, 1819 (2007).

[7] S. A. Khan and K. F. Jensen, Adv. Mater. **19**, 2556 (2007).

[8] H. C. Shum, J. W. Kim, and D. A. Weitz, J. Am. Chem. Soc. **130**, 9543 (2008).

[9] D. K. Hwang, D. Dendukuri, and P. S. Doyle, Lab Chip **8**, 1640 (2008).

[10] A. R. Abate, A. T. Krummel, D. Lee, M. Marquez, C. Holtze, and D. A. Weitz, Lab Chip **8**, 2157 (2008).

[11] H. C. Shum, D. Lee, I. Yoon, T. Kodger, and D. A. Weitz, Langmuir **24**, 7651 (2008).

[12] D. Lee and D. A. Weitz, Adv. Mater. **20**, 3498 (2008).

[13] B. Wang, H. C. Shum, and D. A. Weitz, ChemPhysChem **10**, 641 (2009).

[14] C.-H. Chen, R. K. Shah, A. R. Abate, and D. A. Weitz, Langmuir **25**, 4320 (2009).

[15] P. E. Arratia, J. P. Gollub, and D. J. Durian, Phys. Rev. E **77**, 036309 (2008).

[16] K. Hosokawa, T. Fujii, and I. Endo, Anal. Chem. **71**, 4781 (1999).

[17] B. Zheng, J. D. Tice, L. S. Roach, and R. F. Ismagilov, Angew. Chem., Int. Ed. **43**, 2508 (2004).

[18] J. A. Schwartz, J. V. Vykoukal, and P. R. C. Gascoyne, Lab Chip **4**, 11 (2004).

[19] D. N. Breslauer, P. J. Lee, and L. P. Lee, Mol. Biosyst. **2**, 97 (2006).

[20] H. Song, D. L. Chen, and R. F. Ismagilov, Angew. Chem., Int. Ed. **45**, 7336 (2006).

[21] D. B. Weibel and G. M. Whitesides, Curr. Opin. Chem. Biol. **10**, 584 (2006).

[22] K. Ahn, C. Kerbage, T. P. Hunt, R. M. Westervelt, D. R. Link, and D. A. Weitz, Appl. Phys. Lett. **88**, 024104 (2006).

[23] V. Srinivasan, V. K. Pamula, and R. B. Fair, Lab Chip **4**, 310 (2004).

[24] H. Moon, A. R. Wheeler, R. L. Garrell, J. A. Loo, and C. Kim, Lab Chip **6**, 1213 (2006).

[25] A. Huebner, M. Srisa-Art, D. Holt, C. Abell, F. Hollfelder, A. J. deMello, and J. B. Edel, Chem. Commun. **2007**, 1218.

[26] J. Clausell-Tormos, D. Lieber, J. C. Baret, A. El-Harrak, O. J. Miller, L. Frenz, J. Blouwolff, K. J. Humphry, S. Koester, and H. Duan, Chem. Biol. **15**, 427 (2008).

[27] J. F. Edd, D. D. Carlo, K. J. Humphry, S. Koester, D. Irimia, D. A. Weitz, and M. Toner, Lab Chip **8**, 1262 (2008).

[28] B. H. Weigl, R. L. Bardell, and C. R. Cabrera, Adv. Drug Delivery Rev. **55**, 349 (2003).

[29] C. H. J. Schmitz, A. C. Rowat, S. Koester, and D. A. Weitz, Lab Chip **9**, 44 (2009).

[30] S. Teh, R. Lin, L. Hung, and A. P. Lee, Lab Chip **8**, 198 (2008).

[31] S. L. Anna, N. Bontoux, and H. A. Stone, Appl. Phys. Lett. **82**, 364 (2003).

[32] P. Garstecki, I. Gitlin, W. DiLuzio, G. M. Whitesides, E. Kumacheva, and H. A. Stone, Appl. Phys. Lett. **85**, 2649 (2004).

[33] M. Joanicot and A. Ajdari, Science **309**, 887 (2005).

[34] P. Garstecki, H. A. Stone, and G. M. Whitesides, Phys. Rev. Lett. **94**, 164501 (2005).

[35] P. Garstecki, M. J. Fuerstman, H. A. Stone, and G. M. Whitesides, Lab Chip **6**, 437 (2006).

[36] T. Thorsen, R. W. Roberts, F. H. Arnold, and S. R. Quake, Phys. Rev. Lett. **86**, 4163 (2001).

[37] J. D. Tice, H. Song, A. D. Lyon, and R. F. Ismagilov, Langmuir **19**, 9127 (2003).

[38] B. Zheng, J. D. Tice, and R. F. Ismagilov, Anal. Chem. **76**, 4977 (2004).

[39] P. Guillot and A. Colin, Phys. Rev. E **72**, 066301 (2005).

[40] J. D. Tice, A. D. Lyon, and R. F. Ismagilov, Anal. Chim. Acta **507**, 73 (2004).

[41] H. Stone, A. Stroock, and A. Ajdari, Annu. Rev. Fluid Mech. **36**, 381 (2004).

[42] A. R. Abate, M. B. Romanowsky, J. J. Agresti, and D. A. Weitz, Appl. Phys. Lett. **94**, 023503 (2009).

[43] Y. Xia and G. M. Whitesides, Annu. Rev. Mater. Sci. **28**, 153 (1998).

[44] A. S. Utada, A. Fernandez-Nieves, H. A. Stone, and D. A. Weitz, Phys. Rev. Lett. **99**, 094502 (2007).

[45] K. B. Migler, Phys. Rev. Lett. **86**, 1023 (2001).

[46] P. Guillot, A. Colin, A. S. Utada, and A. Ajdari, Phys. Rev. Lett. **99**, 104502 (2007).

[47] B. Dollet, W. van Hoeve, J. P. Raven, P. Marmottant, and M. Versluis, Phys. Rev. Lett. **100**, 034504 (2008).

[48] P. Guillot, A. Colin, and A. Ajdari, Phys. Rev. E **78**, 016307 (2008).

[49] K. J. Humphry, A. Ajdari, A. Fernandez-Nieves, H. A. Stone, and D. A. Weitz, Phys. Rev. E **79**, 056310 (2009).

[50] See EPAPS Document No. E-PLEEE8-80-089908 for movies of drop formation for different drop makers and flow conditions. For more information on EPAPS, see http://www.aip.org/pubservs/epaps.html.

[51] J. Eggers and E. Villermaux, Rep. Prog. Phys. **71**, 036601 (2008).

[52] P. Garstecki, A. M. Ganan-Calvo, and G. M. Whitesides, Bull. Pol. Acad. Sci.: Tech. Sci. **53**, 361 (2005).